Appl. Magn. Reson. 21, 275–286 (2001)

Applied Magnetic Resonance

Transfer Matrix Method for Optimizing Quasioptical EPR Cavities

K. A. Earle[1], R. Zeng[2], and D. E. Budil[2]

[1] Department of Chemistry and Chemical Biology, Cornell University, Ithaca, New York, USA
[2] Department of Chemistry, Northeastern University, Boston, Massachusetts, USA

Received July 10, 2001

Abstract. We present a convenient method for characterizing and optimizing the performance of quasioptical electron paramagnetic resonance (EPR) sample cavities. The formalism is based on the transfer matrix method used in transmission line analysis. Transfer matrix representations are defined for each of the essential components of an open resonator, and the method is demonstrated by application to selected practical examples. Emphasis is given to optimization of quasioptical EPR for aqueous biological samples.

1 Introduction

One of the major obstacles in the application of high-field electron paramagnetic resonance (EPR) to biological samples near physiological temperatures has been a lack of sensitivity with respect to aqueous samples. This is largely due to the fact that water exhibits significant dielectric losses at micro- and millimeter-wave frequencies. Researchers at high field have encountered significant difficulties in observing spins in aqueous samples with sensitivity comparable to conventional EPR. Such difficulties occur despite the fact that the dielectric loss tangent of water generally decreases with frequency above 20 GHz. However, at higher frequencies it is still necessary to minimize losses by ensuring that even small aqueous sample volumes are not in contact with the E field in a resonator. The need to decrease the sample thickness at smaller λ thus to some degree offsets the gain in sensitivity that might be expected with lower dielectric losses.

Barnes and Freed [1] have described a cell design for aqueous samples consisting of a thin layer of water sandwiched between two dielectric windows mounted transversely in an FPI. A similar sample cell has been applied at 220 GHz by Cardin et al. [2]. Barnes and Freed [1] carried out a detailed analysis on the basis of transmission line reflection coefficients to model the properties of the cell and found that the spectrometer sensitivity depended strongly upon sample geometry, especially the thickness of the aqueous layer. It has proved possible

to design sample cells for a Fabry-Perot transmission cavity that afforded an absolute sensitivity of 10^8 spins/Gauss under favorable conditions [3], which is adequate for studies of many aqueous samples of biological interest. However, the details of the analytical methods used to optimize the cavity have not yet been published.

In the present paper, we present an alternative design method to that utilized by Barnes and Freed [1] for analyzing the sensitivity of different aqueous sample cells in a Fabry-Perot cavity. It is based on the transfer matrix method originally developed for analyzing transmission lines [4, 5], and it relies on the fact that individual Gaussian modes propagating through space are reasonably well represented as waves on a transmission line [6]. The formalism is easy to use and can readily be applied to optimization of sample cells with polar solvents other than water, as well as for a wide variety of dielectric window materials.

2 Theory and Method

In the transfer matrix formalism, an optical element or a system of elements that acts as a linear two-port device may be represented by a general two-by-two matrix **M**. The input and output voltages and currents of the device are then related as follows:

$$\begin{pmatrix} V_{\text{out}} \\ I_{\text{out}} \end{pmatrix} = \mathbf{M} \begin{pmatrix} V_{\text{in}} \\ I_{\text{in}} \end{pmatrix} = \begin{pmatrix} A & B \\ C & D \end{pmatrix} \begin{pmatrix} V_{\text{in}} \\ I_{\text{in}} \end{pmatrix}. \tag{1}$$

The quantities A, B, C, and D are determined by the impedance characteristics of the device. A useful property of this representation is that the output current and voltage for a given element are identical with the input current and voltage of the next element. Thus, a series of optical or circuit elements may be represented by a single matrix that is the product of the matrices for each successive element.

Only two types of matrices are needed to represent a wide variety of open-cavity configurations. The first matrix is used to represent a partially reflective mirror such as a wire grid, a mesh, or a solid mirror with a coupling aperture. Such a mirror is equivalent to a shunt impedance Z_{m} across a transmission line, which has the matrix representation [5, 7–11]

$$M_{\text{m}}(Z_{\text{m}}) = \begin{pmatrix} 1 & 0 \\ 1/Z_{\text{m}} & 1 \end{pmatrix}. \tag{2}$$

The value of Z_{m} is typically small [6] and is purely reactive (i.e., $Z_{\text{m}} = \text{i}X_{\text{m}}$) for perfect (i.e., loss-free) mirrors. A complex-valued impedance can be used to account for such effects as radiation losses, scattering into other modes, diffraction from an aperture or resistive losses in the metal of the mirror.

The second type of matrix is needed to represent transmission of a beam over a given distance through a medium with known dielectric properties. The general form for a matrix $\mathbf{M}_d$ representing a dielectric layer is

$$\mathbf{M}_d(\varepsilon,\mu,d) = \begin{pmatrix} \cosh ik_0 d\sqrt{\mu\varepsilon} & \sqrt{\frac{\mu}{\varepsilon}}\sinh ik_0 d\sqrt{\mu\varepsilon} \\ \sqrt{\frac{\varepsilon}{\mu}}\sinh ik_0 d\sqrt{\mu\varepsilon} & \cosh ik_0 d\sqrt{\mu\varepsilon} \end{pmatrix}, \tag{3}$$

where $k_0 = 2\pi/\lambda_0$ is the wave number of the radiation in free space, d is the path length through the material, $\varepsilon = \varepsilon_v(1 + \chi_e)$, where χ_e is the electric susceptibility of the medium and ε_v is the vacuum permittivity, equal to $8.85 \cdot 10^{-12}$ F/m. In the presence of an EPR-active sample, $\mu = \mu_0(1 + \chi)$, where $\mu_0 = 4\pi \cdot 10^{-7}$ H/m is the vacuum permeability and χ is the EPR sample susceptibility. For propagation through free space, $\varepsilon = \varepsilon_v$ and its permeability is $\mu = \mu_0$. The matrix in Eq. (3) may be applied to dielectric sample cell windows and free space as well as to the sample.

The A, B, C, and D elements of a system matrix $\mathbf{M}_{sys}$ are then used to calculate the field transmission and reflection coefficients of the cavity as follows [12]:

$$r = \frac{E_r}{E_i} = \frac{AZ_{out} + B - CZ_{in}Z_{out} - DZ_{in}}{AZ_{out} + B + CZ_{in}Z_{out} + DZ_{in}},$$

$$t = \frac{E_t}{E_i} = \frac{2Z_{out}}{AZ_{out} + B + CZ_{in}Z_{out} + DZ_{in}}, \tag{4}$$

where E_i, E_r, and E_t are the amplitudes of the incident, reflected, and transmitted fields, and Z_{in} and Z_{out} are the input and output impedances, which are generally both taken to be the impedance of free space, $Z_0 = 377\ \Omega = \sqrt{\mu_0/\varepsilon_v}$.

It should be noted that the field reflection and transmission coefficients are in general complex-valued, since any element in the path introduces a phase shift such that the reflected and transmitted waves are out of phase by $\pi/2$. The power transmission, reflection, and absorption coefficients may be written in terms of the field coefficients: $T = |t|^2$, $R = |r|^2$, and $A = 1 - (T + R)$. To illustrate, applying Eqs. (4) to the transfer matrix for a lossless mirror leads directly to the standard relation between power reflectivity and the imaginary part (reactance) of the effective shunt impedance [12]:

$$R = \frac{Z_0^2}{Z_0^2 + 4X_m^2}. \tag{5}$$

Determining the complex impedance for mirrors with losses requires a knowledge of both reflection and transmission coefficients of the mirror.

To summarize, the approach to analyzing sample cells is to multiply the transfer matrix representations of the different cell components (e.g., mirror, cell

window, liquid layer, free space) according to the given physical configuration. The transmission and reflection coefficients T and R are then determined for the resulting system matrix, and the sensitivity to EPR resonance obtained by taking the partial derivatives of these quantities with respect to the magnetic susceptibility. Sensitivity to the EPR dispersion and absorption signals can be separately determined by taking the derivative with respect to the components χ' and χ'', respectively. Typically the derivative is obtained numerically by a simple forward-differences approximation; i.e., T or R is calculated with χ' or χ'' set to some small number δ (typically on the order of 10^{-6}) then recalculated for $\chi = 0$ and the derivative approximated by $\Delta T/\delta$.

Careful optimization of the sample cell dimensions depends critically on accurate knowledge of ε for the mirrors and window materials as well as the sample solvent in the far-infrared range. A convenient tabulation of ε' and ε'' for a variety of dielectric materials used in the fabrication of quasioptical components at millimeter-wave frequencies has been given by Goldsmith [12]. Extensive measurements of ε have also been tabulated for water as a function of frequency and temperature [13–16]. In general, both ε' and ε'' decrease as the frequency increases above 20 GHz, until resonant absorption bands due to intermolecular librations (as opposed to relaxation processes) begin to occur at around 10 THz [17]. High-frequency dielectric relaxation spectroscopy has also suggested that ε may be significantly altered at millimeter-wave frequencies by the presence of elec-

Table 1. Debye dielectric parameters for a selection of solvents (adapted from ref. 20).

Solvent	Formula	T (°C)	$\varepsilon_0/\varepsilon_v$	$\varepsilon_\infty/\varepsilon_v$	τ (ps)
Water	H_2O	0.0	88.20	5.00	17.7
		10.0	84.00	5.00	16.6
		20.0	80.40	5.20	12.3
		30.0	76.50	5.20	9.3
Sulfuric acid	H_2SO_4	20.0	110.00	5.00	478
Carbon disulfide	CS_2	20.0	2.64	2.65	4.5
Chloroform	$CHCl_3$	25.0	4.72	2.09	7.4
Methanol	CH_3OH	−109.9	82.17	9.80	812
		30.0	31.65	5.50	42.5
Ethanol	C_2H_5OH	−142.6	79	8	$2.65 \cdot 10^6$
		30	23.56	4.2	113
Ethylene glycol	$C_2H_2(OH)_2$	25	41.3	5.4	112
Acetone	C_3H_6O	20	21.2	1.9	3.3
2-Propanol	C_3H_6OH	−95.7	47.1	4	$1.02 \cdot 10^6$
		20	19	3.2	920
Glycerol	$C_3H_5(OH)_3$	−74.6	76.2	4.18	$9.61 \cdot 10^{11}$
		20	34.1	4.8	$1.80 \cdot 10^3$
Ethyl ether	$C_4H_{10}O$	4	4.7	0	2.81
n-Hexane	C_6H_{14}	20	1.89	0	7.43
Cyclohexanone	$C_6H_{10}O$	1	17.01	2.21	14.4
Toluene	C_7H_8	20	2.391	0	7.43
Aniline	$C_6H_5NH_2$	20	6.89	0.028	19.6
Furan	C_4H_4O	20	2.954	0	2.18

trolytes or hydrogen-bonding solutes such as sucrose or glycerol added to promote glass formation [18], as well as the macromolecules themselves [19].

For other solvents of interest, there is often not a tabulation of experimental data available in the 150 GHz to 1 THz frequency range. In such cases it is frequently sufficient to extrapolate measurements made at lower frequencies with the Debye form for dielectric relaxation of the solvent dipole, including possible corrections for sample conductivity:

$$\varepsilon = \varepsilon_\infty + \frac{\varepsilon_0 - \varepsilon_\infty}{1 + \mathrm{i}\omega\tau} - \frac{\mathrm{i}\sigma_0}{\omega\varepsilon_\mathrm{v}}, \tag{6}$$

where ω is the angular frequency at which ε is needed, ε_0 is the static permittivity, ε_∞ is the limiting permittivity at infinite frequency, τ is the rotational correlation time of the solvent, and σ_0 is the DC conductivity of the sample, and ε_v is the permittivity of vacuum defined above. A short compilation of this information for a selection of solvents is given in Table 1 (adapted from ref. 20).

3 Applications and Results

We now apply the formalism described above to characterize the simple quasioptical EPR cavity shown in Fig. 1. This type of cavity is similar to the aqueous sample cell design utilized by Barnes and Freed [1] and by Cardin et al. [2], consisting of two quartz windows of thickness d_w on either side of an aqueous layer of thickness d_s containing the EPR sample. The cell is placed between the mirrors at distances d_1 and d_2 from them. For simplicity, the mirrors are assumed to be planar metal meshes, although in practical implementations at least one of the mirrors is spherical to accommodate Gaussian beams, and the sample is placed as close as possible to the beam waist. Parameters typical of the aqueous sample cells that have been described in the literature are summarized in Table 2; these parameters have been utilized, except as noted, in the calculations presented below.

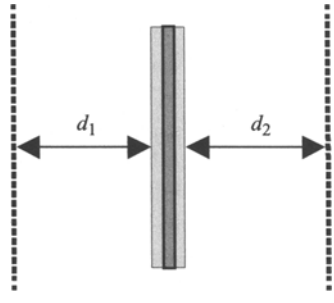

Fig. 1. Schematic diagram of aqueous sample arrangement in a Fabry-Perot resonator. The sample is placed between two dielectric windows located at distances d_1 and d_2 from the partially reflective mirrors of the resonator (dotted lines).

Table 2. Properties of components used for a typical Fabry-Perot cavity with aqueous sample.

Material	$\varepsilon'/\varepsilon_v$	$\varepsilon''/\varepsilon_v$	Thickness d (mm)
Mirror	—	30*	—
Quartz window	4.54	0	0.170
Water	5.5	−6.0	0.017

* Effective $\varepsilon''/\varepsilon_v$ for a normalized impedance of 1/30i.

The matrix product $\mathbf{M}_{cav}$ representing the configuration shown in Fig. 1 is

$$\mathbf{M}_m(Z_m)\mathbf{M}_d(1,1,d_1)\mathbf{M}_d(\varepsilon_w,1,d_w)\mathbf{M}_d(\varepsilon_s,\mu_s,d_s)\mathbf{M}_d(\varepsilon_w,1,d_w)\mathbf{M}_d(1,1,d_2)\mathbf{M}_m(Z_m)\,. \quad (7)$$

Figure 2 shows the power transmission coefficient T calculated as a function of the mirror spacings d_1 and d_2 by applying Eqs. (2)–(4) to the matrix product calculated from Eq. (6) using parameters in Table 2. The peaks observed in the plot correspond to the power transmission maxima that occur when the effective path length through the cavity (taking into account the longer effective path length in the dielectric and sample regions) is near a half-integral number of wavelengths. The plot of R for the same cavity has an analogous, but inverted, appearance, exhibiting minima corresponding to the peaks seen in Fig. 2. The power maxima in the d_1, d_2 space are typically quite elongated, with the approximate long axis of the peak lying parallel to the line $d_1 + d_2 =$ constant.

The curvature of the peaks in Fig. 2 can be understood by examining the transmitted power along lines c and d, as shown in Fig. 3. These lines correspond to translation of the sample with the mirrors fixed at their optimal spacing (c), and spaced further apart than optimal (d). At the optimal spacing, a single, relatively sharp peak is observed. When the mirrors are too far apart, two resonances are observed as the sample is translated through the cavity, each corresponding to a weak resonance between the partially reflective window surfaces and one of the cavity mirrors.

Figure 2 also suggests a preferred approach to tuning Fabry-Perot cavities. It can be seen that motion of either mirror along lines a and a′ will in general produce a series of peaks spaced at $\lambda/2$. Peaks can be observed with the motion of one mirror for a wide range of positions of the other mirror, even far away from the extremum of the peak. To move towards the resonance starting from arbitrary mirror positions thus requires alternating one-mirror adjustments, which can be time-consuming and tedious. The shape and orientation of the transmission peaks suggests that the most efficient motions towards a cavity resonance are along the directions of constant $d_1 + d_2$ and constant $d_1 - d_2$; that is, by first adjusting the mirror spacing with a symmetric motion of the two mirrors, parallel to line b in Fig. 2, and then adjusting the sample location relative to the two mirrors, moving parallel to line c.

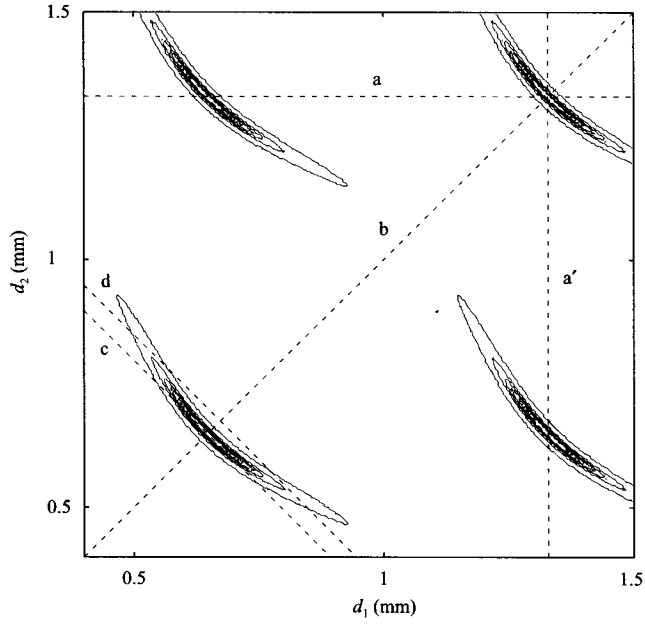

Fig. 2. Power transmission coefficient for the cavity shown in Fig. 1 as a function of mirror spacings d_1 and d_2. Dotted lines correspond to various types of cavity mirror motion: a – motion of one mirror with the other one fixed, b – symmetric motion of the mirrors about the sample, c and d – motion of the mirrors in the same direction, equivalent to motion of the sample relative to fixed mirrors. Calculated with parameters from Table 2, except that Z_m/Z_0 was 0.2 − 4i.

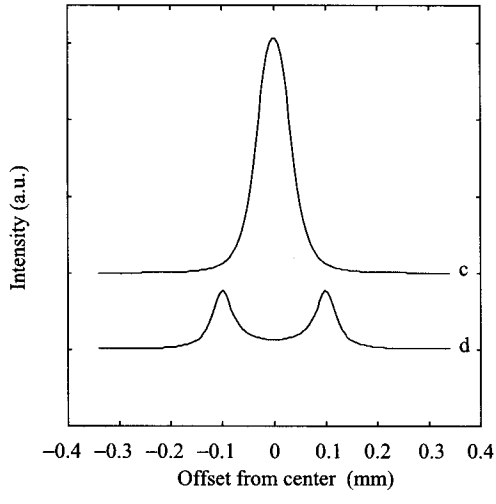

Fig. 3. Transmitted power vs. sample position for translation along each of the dashed lines shown in Fig. 2: c – cavity tuned on resonance, d – cavity off-resonance with mirrors too far apart. Calculated with parameters from Table 2, except that Z_m/Z_0 was 0.2 − 4i.

We now illustrate the use of the transfer matrix method to calculate EPR sensitivity to both absorption and dispersion signals as a function of cavity geometry. Figure 4 shows these quantities for both transmission and reflection cavities, together with transmitted or reflected power. It can be seen that the EPR signal phase is quite sensitive to the mirror spacing and the sample position in both transmission and reflection modes. At the peak of the transmitted power (or minimum in reflected power) and in the absence of any cavity mismatch, the sensitivity to the dispersion signal is zero, and one observes a pure absorption signal. However, relatively small displacements of either the sample or the mirrors can significantly increase the sensitivity to the dispersion signal, resulting in an effective phase shift in the observed EPR signal.

Figure 5a demonstrates sample cavity optimization for solvents with different dielectric properties with a fixed window thickness of 0.17 mm. Calculations of sensitivity to χ'' as a function of sample thickness were carried out for water, methanol, ethanol, and toluene in order to illustrate cavity behavior for both polar and nonpolar solvents. For each curve, the window spacing was adjusted to maximize EPR sensitivity at every value of the sample thickness with a one-dimensional search algorithm [21]. All of the curves exhibit a maximum as the

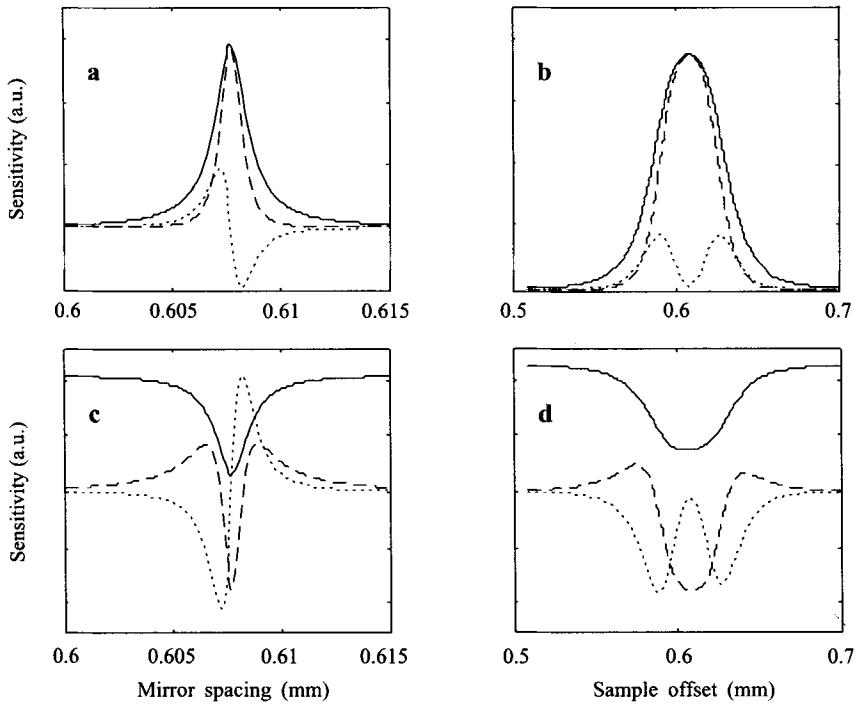

Fig. 4. Millimeter-wave power (solid lines) and EPR sensitivity to absorption (dashed lines) and dispersion (dotted lines) for mirror displacements (**a** and **c**) and sample displacements (**b** and **d**) for transmission (**a** and **b**) and reflection (**c** and **d**) modes. Calculated with parameters given in Table 2.

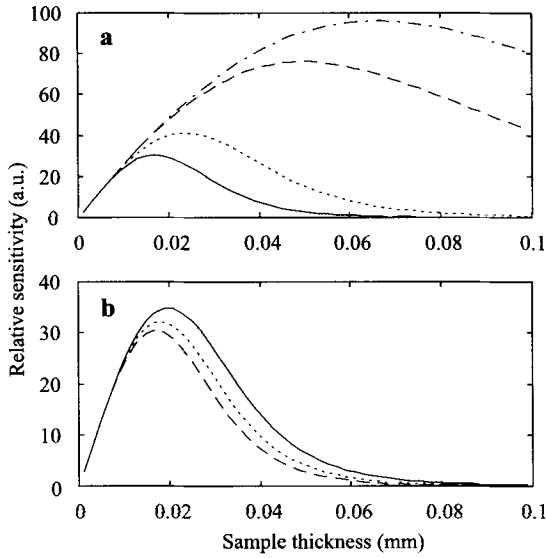

Fig. 5. EPR sensitivity as a function of sample thickness for various solvents with a fixed window thickness of 0.17 mm. **a** Sensitivity curves for solvents of different polarity: water (solid line), methanol (dotted line), ethanol (dashed line), and toluene (dot-and-dashed line). **b** Sensitivity curves for water at different temperatures: 20°C (solid line), 10°C (dotted line), and 0°C (dashed line). Calculated with parameters given in Tables 1 and 2.

sample thickness increases, reflecting the competing effects of increasing the number of spins in the sample and attenuation of the millimeter-wave power through dielectric losses in the sample. For the thinnest samples, the sensitivity is limited by the number of spins; thus, sensitivity increases linearly with sample thickness and does not depend strongly on the dielectric properties of the sample. Since dielectric losses have a logarithmic dependence upon sample thickness (cf. the hyperbolic functions in Eqs. (3)), they become dominant as the sample thickness increases. Thus, lossy samples exhibit a maximum at smaller thickness, whereas the linear increase in sensitivity occurs over a significantly larger range of thickness for low-loss solvents such as toluene, leading to a maximum at larger sample thickness and substantially greater sensitivity.

It is frequently necessary to carry out temperature-dependent studies or freeze an aqueous sample in order to determine its magnetic parameters from the rigid limit spectrum before applying line shape analysis to liquid solution spectra. However, under certain circumstances, rather large changes in sensitivity can occur with relatively small changes in temperature for aqueous samples. This effect is illustrated in Fig. 5b, which shows EPR sensitivity as a function of sample thickness for an aqueous sample at three different temperatures. For samples slightly thicker than the optimum value, the sensitivity can decrease by a factor of two upon cooling from room temperature to the freezing point, even neglecting the inevitable changes in the sample volume and cavity dimensions

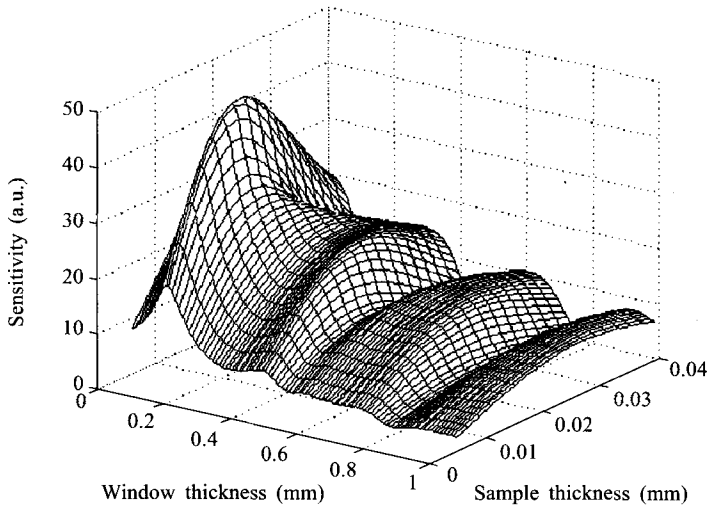

Fig. 6. EPR sensitivity as a function of window and sample thickness calculated with the transfer matrix method with the parameters given in Table 2.

with temperature. In contrast, the sensitivity is relatively unaffected for samples slightly thinner than the optimum value, suggesting that this is a better choice for the sample thickness in temperature-dependent studies of aqueous systems.

To date, most quasioptical EPR spectroscopy on aqueous samples has been carried out with fused quartz microscope cover slips (ESCO Products, Inc., Oak Ridge, NJ) that are about 0.16–0.17 mm in thickness [1, 2]. However, as the plot of EPR sensitivity vs. window and sample thickness in Fig. 6 shows, this is not the optimal value for aqueous samples, although it affords sensitivity within about 50–75% of the maximum. The convenience and ready commercial availability of such windows as well as the difficulty in handling thinner dielectrics have reduced incentives to develop sample cells with thinner windows for regular use. Moreover, Fig. 6 indicates a secondary maximum at window thickness near 0.45 mm that yields sensitivity comparable to that from the 0.17 mm cover slips, but with somewhat greater sample layer thickness. Windows of this thickness would be less fragile, although substantially more expensive to manufacture.

Finally, we illustrate the use of the transfer matrix formalism to calculate quantities such as Q factors and coupling parameters that are familiar to EPR spectroscopists from the equivalent circuit description of EPR cavities. Estimation of these parameters requires knowledge of the effective impedance of the cavity contents, i.e., the free space-window-sample-window-free space elements between the mirrors. In order to find this quantity, one first forms the transfer matrix product of the cavity contents,

$$\mathbf{M}_{\text{cont}} = \mathbf{M}_{\text{d}}(1, 1, d_1)\,\mathbf{M}_{\text{d}}(\varepsilon_{\text{w}}, 1, d_{\text{w}})\,\mathbf{M}_{\text{d}}(\varepsilon_{\text{s}}, \mu_{\text{s}}, d_{\text{s}})\,\mathbf{M}_{\text{d}}(\varepsilon_{\text{w}}, 1, d_{\text{w}})\,\mathbf{M}_{\text{d}}(1, 1, d_2)\,. \quad (8)$$

The input impedance of any transmission line element or equivalent element that is terminated with output impedance Z_{out} is given in terms of its representative transfer matrix elements as

$$Z_{in} = \frac{AZ_{out} + B}{CZ_{out} + D}. \tag{9}$$

The impedance "seen" by the input mirror (an arrangement suitable for a reflection mode resonator) is then the effective impedance of the cavity contents when terminated by a perfectly reflecting short ($Z_{out} = 0$):

$$Z_{eff} = \frac{B}{D}. \tag{10}$$

The unloaded cavity quality factor Q_U can be estimated directly from Z_{eff}:

$$Q_U = \frac{\mathrm{Im}\{Z_{eff}\}}{\mathrm{Re}\{Z_{eff}\}},$$

and the coupling parameter β for the mirror obtained from the mirror impedance and effective cavity impedance as follows [10]:

$$\beta = \frac{|X_m|^2}{Z_0 \,\mathrm{Re}\{Z_{eff}\}}. \tag{11}$$

These quantities can then be used to calculate the loaded quality factor of the cavity, Q_L. For a transmission cavity, the coupling parameters will be different if their reflectivities differ, or if the cavity elements are disposed asymmetrically. In order to apply the transfer matrix formalism to the transmission mode case, we replace the short ($Z_{out} = 0$) in Eq. (9) with a second shunt reactance in parallel with the characteristic impedance of the output transmission line, Z_0.

In the case of a transmission cavity [5, 11],

$$Q_L = \frac{Q_U}{1 + \beta_1 + \beta_2}. \tag{12}$$

For a reflection cavity β_2 is taken to be zero. Thus, the transfer matrix formalism can be used to calculate quantities that allow direct comparison with other types of sample cavity.

4 Conclusion

The transfer matrix method used in transmission line analysis has been demonstrated for quasioptical EPR cavities at high fields. The method is straightforward and easy to apply even to complex cavity configurations. A number of practical examples have been given to illustrate optimization of quasioptical EPR

cavities containing aqueous samples typical of biological systems, and to illustrate their behavior with respect to the phase of the EPR signal. The method enables direct correlation with equivalent circuit parameters for the cavity that are familiar from conventional waveguide-based EPR.

Although the examples were limited in the main to simple, symmetric transmission cavities, the method may readily be extended to asymmetric cavities in the reflection mode, as discussed above. Significant increases of sensitivity in the reflection mode over cavity configurations currently in use may be expected. Readers interested in the details of the methods used may find the Matlab [22] routines used in our calculations at the following URL: ftp://millie.chem.neu.edu/pub/transmatrix.

Acknowledgements

This work was supported by NSF award MCB 9600940 (DEB) and CHE 9615910 and NIH grant RR07126-07 (KAE).

References

1. Barnes J.P., Freed J.H.: Rev. Sci. Instrum. **68**, 2838–2846 (1997)
2. Cardin J.T., Kolaczkowski S.V., Anderson J.R., Budil D.E.: Appl. Magn. Reson. **16**, 273–292 (1999)
3. Earle K.A., Freed J.H.: Appl. Magn. Reson. **16**, 247–272 (1999)
4. Collin R.E.: Foundations for Microwave Engineering, 2nd edn. New York: McGraw-Hill 1992.
5. Budil D.E., Ding Z., Smith G.R., Earle K.A.: J. Magn. Reson. **144**, 20–34 (2000)
6. Born M., Wolf E.: Optics, 6th edn. Oxford: Pergamon Press 1980.
7. Lesurf J.C.G.: Millimetre-Wave Optics, Devices, and Systems. Bristol: Adam Hilger 1990.
8. Ulrich R.: Infrared Phys. **7**, 37–55 (1967)
9. Goldsmith P.F. in: Infrared and Millimeter Waves (Button K., ed.), vol. 6, pp. 277–344. New York: Academic Press 1982.
10. Montgomery C.G., Dicke R.H., Purcell E.M.: Principles of Microwave Circuits. New York: McGraw-Hill 1948.
11. Harvey A.F.: Microwave Engineering. New York: Academic Press 1963.
12. Goldsmith P.F.: Quasioptical Systems. Piscataway, NJ: IEEE Press/Chapman and Hall 1998.
13. Barthel J., Bachhuber K., Buchner R., Hetzenauer H.: Chem. Phys. Lett. **165**, 369 (1990)
14. Hasted J.B., Husain S.K., Frescura F.A.M., Birch J.R.: Chem. Phys. Lett. **118**, 622–625 (1985)
15. Hasted J.B., Husain S.K., Frescura F.A.M., Birch J.R.: Infrared Phys. **27**, 11–15 (1987)
16. Afsar M.N., Hasted J.B.: J. Opt. Soc. Am. **67**, 902–904 (1977)
17. Hasted J.B.: Aqueous Dielectrics. London: Chapman and Hall 1973.
18. Wei Y.Z., Sridhar S.J.: Chem. Phys. **92**, 923–928 (1990)
19. Wei Y.Z., Sage J.T., Tian W.D., Kumbharkhane A.C., Sadeghi M., Champion P.M., Sridhar S., McDonald M.J.: J. Phys. Chem. **98**, 6644–6651 (1994)
20. Buckley F., Maryott A.A.: Tables of Dielectric Dispersion Data for Pure Liquids and Dilute Solutions. Washington, D.C.: National Bureau of Standards 1958.
21. Press W.H., Teukolsky S.A., Vetterling W.T., Flannery B.P.: Numerical Recipes in C: The Art of Scientific Computing, 2nd edn. New York: Cambridge University Press 1992.
22. The Math Works, I. MATLAB, 5.3.1 edn. Natick, MA: The Math Works, Inc. 1998.

Authors' address: David E. Budil, Department of Chemistry, Northeastern University, Boston MA 02115, USA
E-mail: dbudil@neu.edu